ION BOMBARDMENT CHARACTERISTICS DURING THE GROWTH OF OPTICAL FILMS USING A COLD CATHODE ION SOURCE

O. Zabeida, J.E. Klemberg-Sapieha, and L. Martinu, *Ecole Polytechnique, Department of Engineering Physics and Materials Engineering, Montreal, Quebec, H3C 3A7, Canada;* and **D. Morton**, *Denton Vacuum LLC, Moorestown, NJ*

KEYWORDS: Ion energy analysis, IBAD, TiO_2, Ta_2O_5.

ABSTRACT

In the present work, the energy and flux of impinging ions are evaluated in the context of ion-assisted deposition of optical films and ion-induced modification of polymer surfaces for improved adhesion. The experiments were performed in a vacuum system equipped with a broad beam cold cathode ion source. The ion energy distribution functions were measured using a multigrid retarding field analyzer for discharges excited in different gases such as O_2, Ar, and N_2. The ion beam characteristics, namely the maximum ion energy, the mean ion energy, and the ion flux, were correlated with the properties of Ta_2O_5 and TiO_2 layers deposited by e-beam evaporation assisted by an oxygen ion beam. These different materials were analyzed by spectroscopic ellipsometry, spectrophotometry, and profilometry. Their optical and mechanical behavior, such as refractive index and stress, are correlated with the evolution of the film microstructure.

1. INTRODUCTION

Ion bombardment is very important in the growth of films and modification of surfaces; it leads to resputtering, knock-in effects, subplantation, breakage of chemical bonds in polymers, etc. [1-3]. We have recently constructed and tested a versatile multigrid retarding field ion energy analyzer (IEA) for the determination of ion energy distribution functions (IEDFs) in vacuum processing systems: It has been applied for the characterization of microwave (MW) (pulsed and continuous), radio-frequency (rf), and dual mode MW/rf plasmas [4, 5], as well as for a magnetron sputtering system [6]. IEDFs of nitrogen ions for the cold cathode ion source were also analyzed in the context of polymer treatment [7]. In the present work we systematically evaluate, using the IEA, the ion characteristics of a broad beam cold cathode ion source, and we relate them to the properties of optical coatings such as TiO_2 and Ta_2O_5, fabricated by ion beam assisted deposition (IBAD).

2. EXPERIMENTAL SETUP

A broad-beam ion source (CC-105, Denton Vacuum, LLC) was installed in a 75 cm diameter stainless steel ion plating system ("Integrity-29", Denton Vacuum, LLC). This ion source is a smaller variant of the cold cathode ion source described earlier [8]. The ion beam characteristics are controlled by the discharge current (drive current), I_D, and by the potential between the ring anode and the grounded cathode (drive voltage), V_D; the latter parameter creates an electric field necessary to ionize the gas species. The magnetic field from permanent magnets improves the electron confinement, and it allows one to ignite the discharge at relatively low pressures in the reactor. A hot-filament neutralizer was used to avoid surface charging and arcing, and it also served as an additional source of electrons to stabilize the discharge. A pumping speed of 1500 l/s (cryopump) allowed us to maintain the reactor pressure between $1 \cdot 10^{-4}$ and $4 \cdot 10^{-4}$ Torr, while using gas flow rates of 10-50 sccm of Ar, O_2, and N_2, required for proper functioning of the ion source.

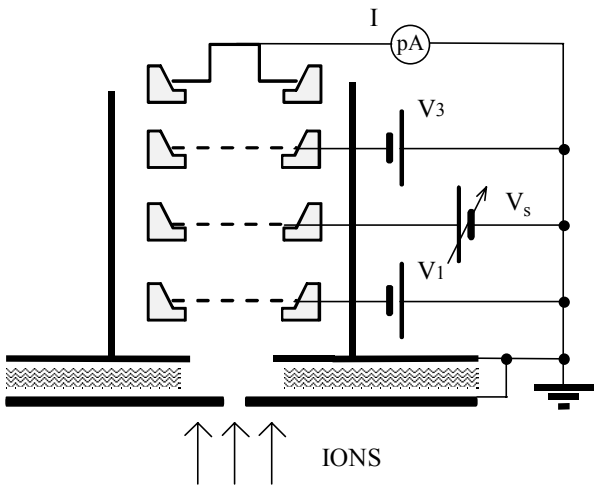

Figure 1. *Schematic representation of the ion energy analyzer.*

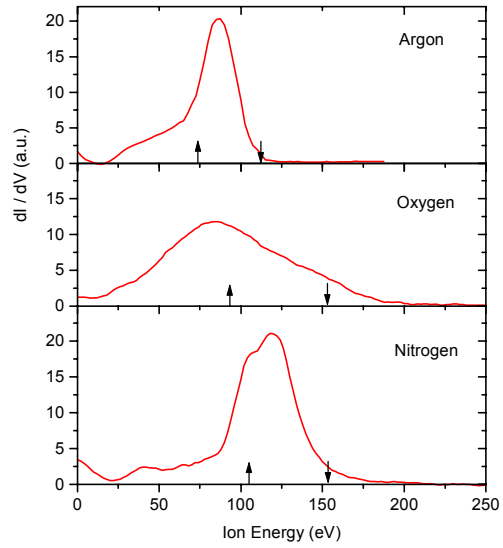

Figure 2. *IEDFs measured for different working gases. I_D is 2 A , pressure is $3 \cdot 10^{-4}$ Torr and the angle from the source axis is 22.5° for all presented curves. Here and in all other IEDFs in this article, upward and downward pointing arrows indicate $\langle E_i \rangle$ and V_D, respectively.*

The IEDFs were measured with a retarding field, three-grid ion energy analyzer [4] illustrated in Figure 1. For the pressure range used in this work no differential pumping was necessary. The IEA was placed at a distance of 0.5 m from the source in three different positions (0°, 22.5° and 45°) with respect to the ion source axis. The IEDFs were obtained by derivation of the $I(V_s)$ characteristic, where I is the collector current (see Figure 1) and V_s is the scanning potential (both of them were controlled by a computer) [4]. Energy resolution of the IEA is about 2 eV.

Thin titanium oxide and tantalum oxide films were deposited by electron beam evaporation of the respective metals in an oxygen atmosphere, assisted by oxygen ion bombardment from the cold cathode ion source.

The refractive index and thickness of films were determined from the measurements using a variable angle spectroscopic ellipsometer (VASE, J.A. Woollam Co., Inc.) and a spectrophotometer (Lambda 9000, Perkin Elmer). The film stress was determined by a curvature method using laser interferometry (Flexus, Tencor). In order to evaluate the film structural stability, selected specimens were annealed to 400 °C and 800 °C in laboratory air.

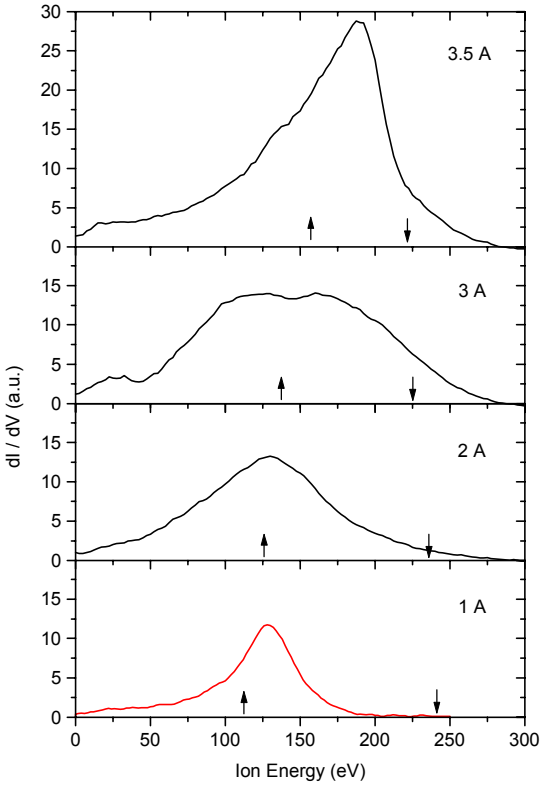

Figure 3. *IEDFs for different I_D values at an oxygen pressure of $2 \cdot 10^{-4}$ Torr.*

3. RESULTS AND DISCUSSION

3.1. Ion energy distributions

Typical IEDFs, measured for three frequently used gases, namely argon, nitrogen, and oxygen, at the same pressure of 0.3 mTorr and I_D = 2 A are shown in Figure 2. Depending on the gas nature, the distributions exhibit different shapes. One should keep in mind that the process conditions for each gas slightly varied: in the case of argon, a lower drive voltage, 115 V, is applied, compared to 155 V for oxygen and nitrogen, as a consequence of a higher ionization rate in argon compared to molecular gases. On the other hand, in the case of nitrogen and oxygen all external parameters were almost identical; nevertheless, the IEDF for oxygen is much broader and it is shifted to lower energies. This difference can be attributed to negative ion formation in oxygen plasma that changes the plasma potential distribution in the source. Access to the IEDF allowed us to evaluate for each set of experimental conditions an important process parameter, namely the mean ion energy, $\langle E_i \rangle$, using the following expression:

$$\langle E_i \rangle = \frac{\int E \cdot f_i(E) dE}{\int f_i(E) dE} . \qquad (1)$$

Here $f_i(E)$ represents the specific IEDF.

Since oxygen is frequently used in the fabrication process of optical coatings, we particularly focused on the

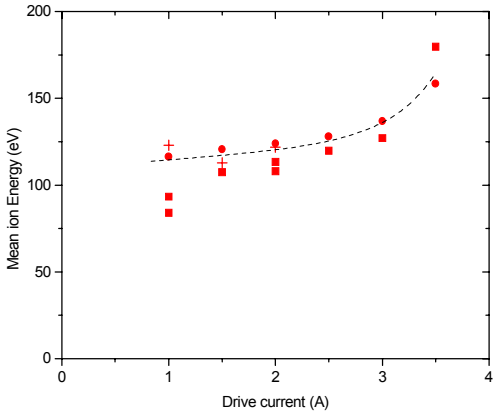

Figure 4. *Mean ion energy as a function of drive current for different angles with respect to ion source axis: triangles- 0º, squares - 22.5º, and circles- 45º.*

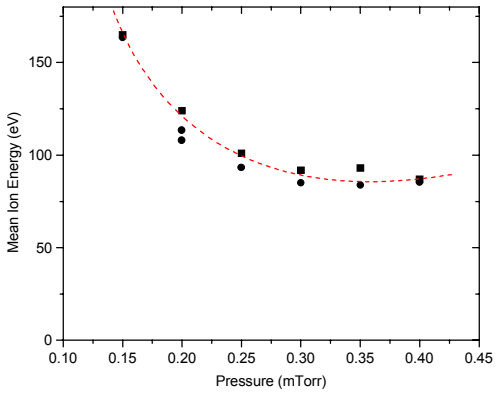

Figure 6. *Mean ion energy as a function of pressure for different angles with respect to ion source axis: squares - 22.5º, circles- 45º.*

ion characteristics in this gas. Figure 3 represents the IEDFs for oxygen at a pressure of 0.2 mTorr but at different I_D values. Increasing I_D leads to broadening of the IEDF, while the ion current density increases substantially. $\langle E_i \rangle$ is shown in Figure 4 as a function of I_D for different angles with respect to the source axis. $\langle E_i \rangle$ values monotonously increase; less variation in $\langle E_i \rangle$ was observed for I_D between 1.5 and 2.5 A. We conclude that the drive current allows one to control the ion flux during deposition while keeping the mean ion energy essentially the same. The IEDFs measured for different angles with respect to the ion source axis yield $\langle E_i \rangle$ values and intensities very close to each other, which confirms a beam uniformity of about 10 % over the measured area (~0.5 m^2 assuming axial symmetry).

The effect of pressure on the IEDFs of oxygen ions is shown in Fig. 5. Two effects are observed to occur when the pressure increases: (i) the drive voltage decreases leading to the observed drop in $\langle E_i \rangle$ as illustrated in Figure 6; (ii) the ion current (area under the curves) drops, in agreement with the Child-Langmuir law ($I \propto U^{3/2}$). It is believed that this effect interferes with changes in the shape of the plasma edge, from which the ions are extracted (plasma expansion at lower pressure). In contrast to nitrogen ions [7] no IEDF broadening due to ion-neutral collisions has been observed here.

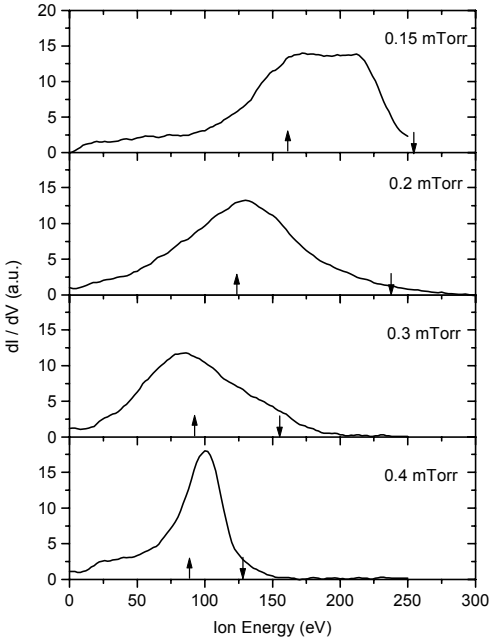

Figure 5. *IEDFs for different oxygen pressure values at I_D = 2 A.*

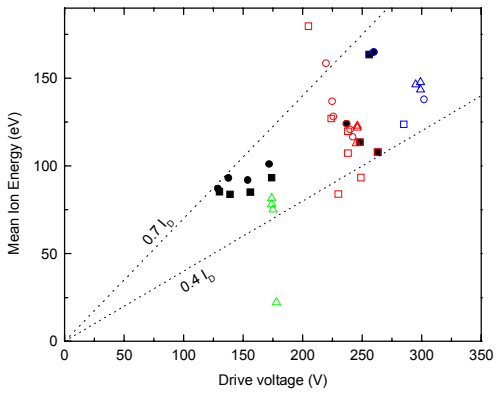

Figure 7. *Mean ion energy as a function of drive voltage for different angles with respect to ion source axis: triangles- 0º, squares - 22.5º, circles- 45º.*

In the case of oxygen, IEDFs are narrower, which may also be attributed to geometrical changes of the extraction zone. It is intuitively expected that V_D is a parameter most closely related to the ion energy. Indeed, as one can see in Fig. 7, the $\langle E_i \rangle$ values derived from almost all IEDFs obtained over a large range of drive currents (0.5-4

Table 1. Conditions of film deposition and film characteristics.

Film	I_D (A)	V_D (V)	$\langle E_i \rangle$ (eV)	I ($\mu A/cm^2$)	$\langle E_i \rangle$ x I (mW/cm^2)	Film thickness (nm)	n (at 600 nm)	Stress (MPa)
Ta_2O_5	0	0	0	0	0	396	2.09	1
	1	224	115	28	3.2	341	2.07	99
	2	284	126	57	7.2	322	2.12	98
	3	264	138	90	12.3	306	2.16	78
TiO_2	0	0	0	0	0	418	2.15	176
	1	244	115	28	3.2	365	2.26	214
	2	308	126	57	7.2	305	2.39	183
	3	278	138	90	12.3	297	2.44	-391

A) and gas pressures ($1.5\text{-}4.0\cdot10^{-4}$ Torr) lie between $0.4\cdot eV_D$ and $0.7\cdot eV_D$. Therefore, a value of $0.5\cdot eV_D$ can serve as a good approximation of $\langle E_i \rangle$ for the ion source studied in this work.

Due to principal limitations of our IEA, we cannot distinguish either single- or double-charged ions, or ions with different masses. This lack of information somewhat complicates the interpretation of the IEDFs in molecular gases. Presence of ions with higher energies than those corresponding to the drive voltage (see Figures 2, 3, and 5), points to charge transfer in which double-charged and molecular ions can participate. Our recent mass-resolved measurements of IEDFs in nitrogen rf and MW plasmas clearly prove this statement [9].

3.2 Film analysis

We studied the effect of ion energy and ion flux on the refractive index, the deposition rate and the internal stress of TiO_2 and Ta_2O_5 films, and the results are summarized in Table 1. Clearly, a higher ion flux gives rise to material densification, accompanied by a decrease of the deposition rate and an increase of the refractive index, in agreement with an abundant literature on this subject (e.g., [1]).

As discussed in [3], the effect of ion bombardment on the evolution of the film microstructure can be described by a single parameter, E_p, namely the energy delivered to the film per deposited atom:

$$E_p = \langle E_i \rangle \cdot \Phi_i / \Phi_n \qquad (2)$$

Here Φ_i is the ion flux and Φ_n is the flux of condensing atoms. Equation 2 is a simplified version of a more complex description of ion-assisted phenomena [10].

Evolution of the TiO_2 and Ta_2O_5 film characteristics is shown plotted in Figure 8 as a function of E_p. The results indicate that the deposition rate for both films decreases with E_p as a consequence of densification at higher energy fluxes toward the film. The stress is relatively low (0 - 200 MPa), and it is tensile for lower E_p values, while one measurement suggests its conversion to a compressive one. The effect of E_p appears to be more significant on the evolution of n values for TiO_2 than for Ta_2O_5. TiO_2 is therefore more sensitive to the E_p variations in the present range of conditions, in agreement with the structure-zone model [1,2].

Selected samples, namely those deposited at the highest and the lowest ion flux and E_p values for both materials, were annealed for one hour at 400 and 800 ºC. The effect on the film thickness, the refractive index and the surface roughness is illustrated in Table 2. Systematically

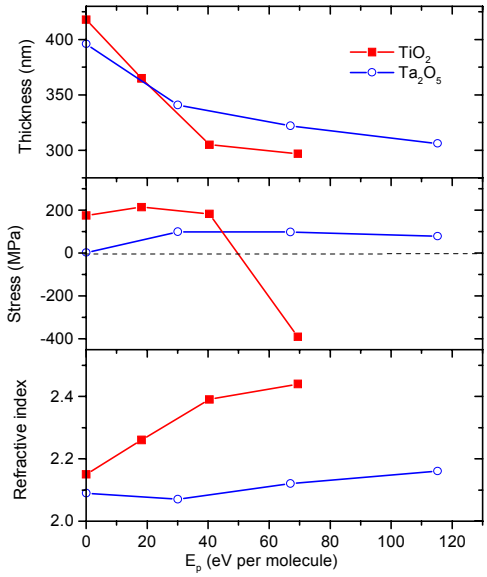

Figure 8. *Film characteristics as a function of total ion energy per deposited molecule.*

higher thickness stability has been found for both materials for the films deposited at high E_p values as expected. It should be mentioned, however, that annealing at 800 ºC was accompanied by a strong increase in surface roughness that

Table 2. Effect of annealing temperature on the optical properties of deposited films.

Film	I_D (A)	Temperature (ºC)	Thickness (nm)	Roughness (nm)	n (at 600 nm)	Mean Square Error
TiO_2	0	20	396	0	2.15	
		400	390	0	2.25	10
		800	382	0	2.26	21
	3	20	306	0	2.44	
		400	298	4.2	2.47	16
		800	282	7.4	2.62	19
Ta_2O_5	0	20	418	0	2.09	
		400	331	2.0	2.09	5
		800	302	15.3	2.20	66
	3	20	297	0	2.16	
		400	302	2.2	2.15	5
		800	282	4.8	2.28	50

may have partially affected the accuracy in determining the refractive index and thickness. Modification of surface morphology appears to be related to a transition from an amorphous to partially crystalline microstructure upon annealing between 400 ºC and 800 ºC, as indicated by our preliminary X-ray diffraction measurements, and also reported by other authors [11]. A more detailed study of structural stability of these films is presently in progress in our laboratory.

4 CONCLUSIONS

The present work has been performed as part of our continued interest in the analysis and control of ion bombardment effects in the growth of thin films. We describe a simple three-grid electrostatic ion energy analyzer we have used for the evaluation of ion energy distribution functions in an IBAD system, equipped with a cold cathode broad beam ion source. Systematic measurements of the IEDFs over a large range of process conditions were performed to determine the mean ion energy and the total ion flux. These values were used to calculate an important process parameter, namely the ion energy per deposited atom, which should be optimized in order to obtain the desired performance of deposited films. Such an approach has been illustrated by the measurements of the characteristics of TiO_2 and Ta_2O_5 optical films.

ACKNOWLEDGMENTS

The authors wish to thank Mr. G. Jalbert for his expert technical assistance, Mr. P. Bellerose for the stress measurements, and Mr. D. Dalacu and Mr. D. Poitras for the evaluation of optical characteristics.

REFERENCES:

1. J.J. Cuomo, S.M. Rossnagel, and H.R. Kaufman, ed., Handbook of Ion Beam Processing Technology, Noyes Publications, Park Ridge, NJ, 1989.
2. S.M. Rossnagel, J.J. Cuomo, and W.D. Westwood, ed., Handbook of Plasma Processing Technology, Noyes Publications, Park Ridge, NJ, 1989.
3. M.R. Wertheimer, L. Martinu, and E.M. Liston, in Handbook of Thin Film Process Technology, IOP Publishing Ltd., Bristol 1996, Chapter E3:0, pp. 1-38.
4. O. Zabeida and L. Martinu, J. Appl. Phys., **85**(9), p. 6366, 1999.
5. O. Zabeida, J.E. Klemberg-Sapieha, and L. Martinu, Proc. 41th Ann. Tech. Conf., Society of Vacuum Coaters, Boston, 1998, p. 336.
6. Unpublished results from our laboratory.
7. O. Zabeida, J.E. Klemberg-Sapieha, L. Martinu, and D. Morton, Proc. 1998 Fall Meeting, Materials Research Society, Boston, 1998.
8. P.R. Denton, J. Lee, and A. Musset, Proc. Ann. Tech. Conf., Society of Vacuum Coaters, Albuquerque, 1985, p.53.
9. A. Hallil, O. Zabeida, J.E. Klemberg-Sapieha, M. Wertheimer, and L. Martinu, Proc. 42 Ann. Tech. Conf., Society of Vacuum Coaters, Chicago, 1999, this volume.
10. L. Martinu, in Plasma Processing of Polymers, Kluwer Academic Publishers, Dordrecht, 1997, p. 247.
11. R. Rujkoran, L. S. Hsu, and C. Y. She, NBS Special Publication 727, p.253, 1985.